REPORT DOCUMENTATION PAGE

Form Approved
OMB No. 0704-0188

PLEASE DO NOT RETURN YOUR FORM TO THE ABOVE ADDRESS.

1. REPORT DATE *(DD-MM-YYYY)*	2. REPORT TYPE	3. DATES COVERED *(From - To)*
03/23/2010	FINAL	04/01/2007-12/31/2010

4. TITLE AND SUBTITLE

DEVELOPMENT OF THE MONACO-PIC CODE FOR 12V CHAMBER PLASMA PLUME ANALYSIS

5a. CONTRACT NUMBER

FA9550-07-1-0274

5b. GRANT NUMBER

5c. PROGRAM ELEMENT NUMBER

6. AUTHOR(S)

IAIN BOYD

5d. PROJECT NUMBER

5e. TASK NUMBER

5f. WORK UNIT NUMBER

7. PERFORMING ORGANIZATION NAME(S) AND ADDRESS(ES)

IAIN BOYD
1320 BEAL AVE
ANN ARBOR, MICHIGAN 48109

8. PERFORMING ORGANIZATION REPORT NUMBER

9. SPONSORING/MONITORING AGENCY NAME(S) AND ADDRESS(ES)

AFOSR
875 N RANDOLPH ST
ARLINGTON VA 22203

10. SPONSOR/MONITOR'S ACRONYM(S)

11. SPONSOR/MONITOR'S REPORT NUMBER(S)

AFRL-AFOSR-VA-TR-2016-0082

12. DISTRIBUTION/AVAILABILITY STATEMENT

DISTRIBUTION A

13. SUPPLEMENTARY NOTES

14. ABSTRACT

The first part of this report discusses the progress made in modeling the plume of a highpower Hall thruster tested within the 12V vacuum test facility located at the Arnold Engineering and Development Center (AEDC), Tullahoma, Tennessee. Over the course of the project, significant progress was made in further development of an existing simulation capability called MONACO. MONACO employs a combination of direct simulation Monte Carlo and Particle-In-Cell methods to compute the plasma flow in 12V. New features added to MONACO include: (1) analysis of solid baffles in 12V; (2) ability to compute plasma flow properties measured by a virtual probe; and (3) implementation of a detailed electron fluid model to describe the plasma. The new features were assessed by direct comparison with data measured during a Hall thruster test conducted in 12V, and the results were found to

15. SUBJECT TERMS

MONACO, solid, AEDC, vacuum, modeling, simulation, highpower, thruster, Monte Carlo

16. SECURITY CLASSIFICATION OF:			17. LIMITATION OF ABSTRACT	18. NUMBER OF PAGES	19a. NAME OF RESPONSIBLE PERSON
a. REPORT	b. ABSTRACT	c. THIS PAGE			Mitat Birkan
					19b. TELEPHONE NUMBER *(Include area code)* 703-696-7234

FINAL TECHNICAL REPORT

Development of the MONACO-PIC Code for 12V Chamber Plasma Plume Analysis

AFOSR GRANT FA9550-07-1-0274

Iain D. Boyd
Department of Aerospace Engineering
University of Michigan
Ann Arbor, MI 48109-2140

Summary

The first part of this report discusses the progress made in modeling the plume of a high-power Hall thruster tested within the 12V vacuum test facility located at the Arnold Engineering and Development Center (AEDC), Tullahoma, Tennessee. Over the course of the project, significant progress was made in further development of an existing simulation capability called MONACO. MONACO employs a combination of direct simulation Monte Carlo and Particle-In-Cell methods to compute the plasma flow in 12V. New features added to MONACO include: (1) analysis of solid baffles in 12V; (2) ability to compute plasma flow properties measured by a virtual probe; and (3) implementation of a detailed electron fluid model to describe the plasma. The new features were assessed by direct comparison with data measured during a Hall thruster test conducted in 12V, and the results were found to be satisfactory. The enhanced MONACO simulation capability has been transferred to AEDC for their future use.

The second part of the report describes progress made in the simulation of a Hall thruster discharge. The need to create an accurate model of the Hall thruster plasma generation was identified as a critical element for achieving accurate plume simulations of the thruster operation in 12V. The plasma discharge model simulates the unsteady behavior of the Hall thruster using a code called HPHALL. While HPHALL has been demonstrated to produce physically accurate results for time-averaged properties such as thruster, there has been little prior work focused on the unsteady results produced by the code. In the work performed in this project, detailed analysis was performed on the unsteady nature of HPHALL results with direct comparisons made with unsteady data measured experimentally.

Part 1-- Modeling of Virtual Diagnostics for Hall Thruster Plumes in a Vacuum-chamber

Nomenclature

e	=	electron charge, 1.6×10^{-19} C
k	=	Boltzmann constant, 1.38×10^{-23} J K^{-1}
n	=	number density, m^{-3}
N	=	number of particles
m	=	mass, kg
T	=	temperature, eV
p	=	pressure, Pa
I_{sp}	=	specific impulse, s
$\vec{v}$	=	velocity, m s^{-1}
g	=	magnitude of relative velocity, m s^{-1}
σ_{EL}	=	collision cross section, m^2
A	=	area, m^2
ω	=	viscosity temperature exponent
σ	=	electrical conductivity, A (V m)$^{-1}$
κ	=	thermal conductivity, W (K m)$^{-1}$
ϕ	=	plasma potential, V
$\vec{E}$	=	electric field, V m^{-1}
$\vec{j}$	=	current density, A m^{-2}
ν	=	collision frequency, s^{-1}
C_i	=	ionization rate coefficient, m^2 s^{-1}
ε_i	=	ionization energy, eV
I_d	=	discharge current, A
V_d	=	discharge voltage, V
ψ	=	electron velocity stream function, m^{-2} s^{-1}

Subscripts

a	=	anode
d	=	discharge
e	=	electron
i	=	ion
s	=	sampling
M	=	Maxwellian
TE	=	thruster exit
VP	=	virtual probe

1.1 Introduction

Hall thrusters are an efficient propulsion option for spacecraft, with high specific impulses making them particularly well suited for low thrust missions. A primary concern regarding the use of Hall thrusters is the effect of their plumes. Possible spacecraft contamination and communications interference emphasizes the importance of plume analysis with regards to spacecraft integration. Two aspects of plume analysis include numerical simulation and ground-based experiments conducted in vacuum chambers. One of these types of facilities is the Arnold Engineering Development Center (AEDC) 12V Vacuum-chamber (see Figure 1). It is the focus of the present work to develop simulation tools that can be applied at AEDC, specifically for the analysis of Hall thruster plumes in 12V.

Hall thruster plume modeling has been reviewed by Boyd[1] where it was determined that hybrid methods are the most successful. In general, the plume of a Hall thruster consists of neutrals, energetic ions, and electrons. Plume behavior is complicated by the multiple types of collisions involved, such as collisions due to thermal velocity and collisions between neutrals and ions with charge exchange, as well as different physical phenomena, such as self-consistent electric fields. Furthermore, in ground-based facilities the presence of a background gas must be accounted for. Computational methods are uniquely suited for plume analysis since different physical models can be interchanged to allow for varying degrees of fidelity.

In this report, hybrid simulation methods are applied to an axisymmetric domain in order to investigate a Hall thruster plume in the 12V vacuum chamber, extending previous work done on the subject.[2, 3] A direct simulation Monte Carlo (DSMC) method[4] is used to model collision dynamics, and a Particle-in-Cell (PIC) method[5] is used to capture electric field effects. Additional capabilities specific to the needs of AEDC are also discussed. Specifically, a virtual probe algorithm is implemented and compared against experimental data taken previously in the 12V chamber for a high power Hall thruster. This algorithm provides a new capability in that current densities at discrete locations can be predicted more accurately. A detailed fluid-electron model[6] is incorporated in place of the standard Boltzmann relation for modeling electrons and is discussed below. Comparisons between the fluid-electron model and Boltzmann relation model are made to determine effects on the calculation of plasma parameters. These comparisons are also extended to determine the effect of the electron model on virtual probe calculations.

1.2 Facility and Thruster

The 12V chamber is a 12-ft diameter vertically oriented vacuum facility at AEDC. The testing considered here was conducted in 12V on 9/13/06 and 9/14/06. Two key features of the facility are the unique geometry and high pumping rates. The geometry is shown in Figure 1. The floors and outer walls of the chamber are liquid nitrogen (LN_2) cooled, held at the cryogenic LN_2 temperature of 77K. The cryo-pumps located at the top and bottom of the chamber are cooled with gaseous helium (GHe), held at the cryogenic GHe temperature of 20K. The chamber has a total pumping rate of about $3\text{-}5\text{x}10^6$ L/s for xenon. This resulted in a back-pressure of 1.4 x 10^{-7} torr for the operating condition under consideration here. The current density measurements utilized in this study were obtained with Faraday cup probes along the chamber centerline. For further details, see Ref. 7.

The thruster tested in this facility was the Busek BHT-20K Hall thruster. The thruster was operated in 12V over a range of conditions including a low I_{sp} , high thrust mode and a high I_{sp} , low thrust mode, the latter being the focus of this work. See Table 1 for the specific operating conditions of the high I_{sp} mode. The BHT-20K is a nominal 20kW input power thruster designed to produce 1.0 N of thrust at 2750 s of I_{sp} and 70% efficiency at optimal operating conditions, as stated in Ref. 8. For further details of BHT-20K operation, see the same reference.

Table 1: BHT-20K Hall thruster operating conditions

Operating Condition	$\dot{m}$	I_d	V_d	ϕ_{ref}
High I_{sp}	19.53 mg/s	21.2 A	500 V	50 V

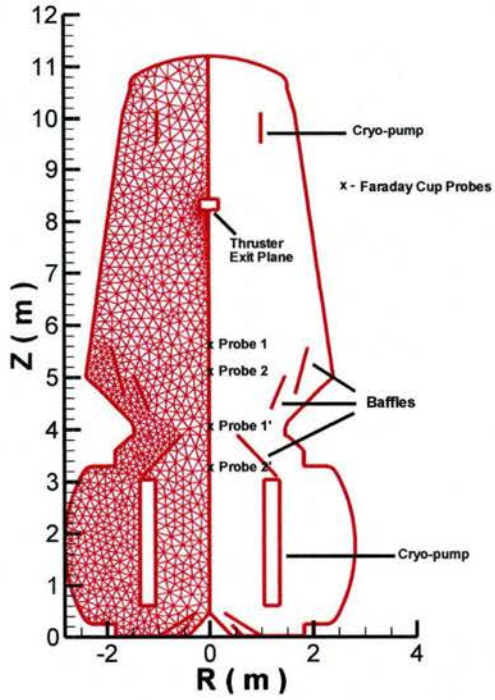

Figure 1: Mesh for the 12V chamber

1.3 Numerical Methods

A. Overview and Collision Dynamics

The numerical simulations use a hybrid DSMC-PIC method to model the plume. The DSMC module handles collisions. The PIC module is used to move the heavier particles that are influenced by the electric fields present. Finally, the electrons are simulated using a fluid model, incorporating either a simple Boltzmann relation or a detailed model.

The DSMC module handles collisions between heavier particles (Xe, Xe^{+}, and Xe^{++}), such as neutral-neutral and ion-neutral collisions. The DSMC method uses virtual particles to simulate collisions in rarefied gas flows. The particles represent real ions and neutrals and are grouped in cells whose characteristic lengths are shorter than a mean free path. Pairs of these particles are selected at random and a collision probability is evaluated that is proportional to the product of the relative velocity and collision cross-section. This probability is compared to a random number to determine if the collision occurs. If so, collision dynamics are performed to alter the properties of the colliding particles. Two types of collision dynamics are relevant to Hall thruster plumes: elastic (momentum exchange) collisions and charge exchange collisions (CEX). Elastic collisions involve only exchange of momentum between participating particles. The Hall thruster plume is confined to two different types of momentum exchange collisions, neutral-neutral collisions and neutral-ion collisions. For neutral-neutral collisions, the variable hard sphere model is employed[4]. The cross-section for xenon is:

$$\sigma_{EL}(Xe,Xe) = \frac{2.12 \times 10^{-18}}{g^{2\omega}}\, m^2 \quad and \quad \omega = 0.12 \tag{1}$$

where g is the relative velocity and ω is related to the viscosity temperature exponent for xenon. For neutral-ion elastic interactions, the cross-sections measured by Miller *et al.*[9] are used:

$$\sigma_{EL}(Xe,Xe^{+}) = (175.26 - 27.2 \log_{10}(g)) \times 10^{-20}\ m^2 \tag{2}$$

$$\sigma_{EL}(Xe,Xe^{++}) = (103.26 - 17.8 \log_{10}(g)) \times 10^{-20}\ m^2 \tag{3}$$

Isotropic scattering is assumed for both types of elastic collisions. Charge exchange collisions pertain to the transfer of one or more electrons between an atom and an ion. These cross sections are assumed to follow the same expressions for neutral-ion elastic collisions. However, it is also assumed there is no transfer of momentum accompanying the charge exchange, since it is primarily a long-range interaction.

B. Plasma Dynamics

The PIC module is used to move the heavier ion particles that are influenced by the electric fields, whereas the lighter electrons are modeled as a fluid. The PIC module determines the charge density at the nodes in the mesh based on the proximity of each particle to the surrounding nodes. The charge density is then used to compute the electric field at each node. This is accomplished either by incorporating the Boltzmann relation or solving for the potential directly using the detailed-fluid model. The potential is then differentiated spatially to obtain the electric fields.

The Boltzmann relation uses several assumptions applied to the electron momentum equation, such as the fluid electron flow being collisionless, isothermal, with no magnetic fields present, and that the electron pressure obeys the ideal gas law, to arrive at the following[10]:

$$\phi = \phi_{ref} + \frac{k T_{ref}}{e} \ln\left(\frac{n_e}{n_{ref}}\right) \tag{4}$$

where ϕ is the plasma potential, ϕ_{ref} is a reference potential, k is Boltzmann's constant, e is the electron charge, T_{ref} is the constant electron reference temperature, and n_e and n_{ref} are the local electron number density and reference electron number density, respectively. Reference values are taken at the thruster exit plane and the parameters used in this study can be found in Table 1. The assumption of quasi-neutrality is employed to obtain the electron number density from the ion number densities.

Most of the strong assumptions made in deriving the Boltzmann relation are questionable in the plume under consideration, especially in the near-field. This is due to strong gradients that could make these approximations inaccurate. Previous work on this subject pointed to increasing the fidelity of physics models to obtain better agreement with experimental results[3]. The detailed electron model first proposed by Boyd and Yim[6] increases the modeling fidelity by removing some of the simplifications made with the Boltzmann relation and modeling the electrons with fluid-type conservation equations. The relations are manipulated into useful forms for numerical

simulation by introducing a stream-function (called the electron velocity potential) for the electron continuity equation and assuming steady state for all the equations. This results in a set of Laplace-type equations with weak source terms, summarized as follows:

$$\nabla^2\psi = n_e n_a C_i \quad \text{where} \quad \nabla\psi = n_e\overrightarrow{v_e} \tag{5}$$

$$\nabla(\sigma\nabla\phi) = \frac{k}{e}\left(\sigma\nabla^2 T_e + \sigma T_e\nabla^2(ln(n_e)) + \sigma\nabla(ln(n_e))\cdot\nabla T_e + T_e\nabla\sigma\cdot\nabla(ln(n_e)) + \nabla\sigma\cdot\nabla T_e\right) \tag{6}$$

$$\nabla^2 T_e = -\nabla(ln(\kappa_e))\cdot\nabla T_e + \frac{1}{\kappa_e}\left(-\vec{j}\cdot\vec{E} + \frac{3}{2}n_e(\overrightarrow{v_e}\cdot\nabla)kT_e + p_e\nabla\cdot\overrightarrow{v_e} + 3\frac{m_e}{m_i}\nu_{ei}n_e k(T_e - T_h) + n_e n_a C_i\epsilon_i\right) \tag{7}$$

This system is treated in the current study in the same manner as in Refs. 11 and 12, the results of which are summarized as follows. By treating the right-hand side as known in Eqs. (5)-(7), three fundamental plasma parameters are solved for, namely $\vec{v}_e$, ϕ, and T_e. This is achieved by expressing the system as a generalized Poisson equation and solving the system with a finite element solver. Derivative calculation is handled by a least squares method, also presented in Ref. 11.

The set of Eqs. (5)-(7) is used twice in the current study. First, the *isothermal detailed model* consists of solving Eqs. (5) and (6), assuming no change in T_e. Second, the *conductivity detailed model* consists in solving Eqs. (5)-(7) keeping only the first source term in (7), in order to ensure the system of equations is weak. The two detailed models increase the level of accuracy by removing some restrictions that the Boltzmann relation assumes, e.g. currentless and isothermal electrons.

C. Boundary Conditions

For computations of a Hall thruster plume in 12V, boundary conditions must be specified at the thruster exit and along all solid surfaces in the computational domain, including cryo-pumps and baffles, for the DSMC-PIC method and for the fluid electron model. First, the boundary conditions for the DSMC-PIC method are presented, followed by those for the fluid electron model.

Some of the macroscopic properties of the plasma are required at the thruster exit, namely the number density, velocity, and temperature of each heavy species in the calculation. Since the particles exit the thruster with an unknown radial velocity component, this results in a velocity vector that is not parallel to the center-line of the chamber. The angle between the center-line and velocity vector is referred to as the divergence angle, and since it is not known a priori, a sensitivity study is performed that includes a range of assumed values. Particles that exit the thruster plane are assigned a radial velocity component that varies linearly with the distance from the center of the thruster channel. Therefore, a particle exiting the center of the channel will have no radial velocity component, while a particle exiting the channel near its inner or outer wall will have the highest radial velocity component and the angle of the velocity vector with respect to the center-line for that particle will be the divergence angle specified.

The other thruster exit macroscopic properties are determined in general via a combination of analysis and estimation in order to match experimental operating conditions in the same manner as Ref. 3. The resulting DSMC-PIC input parameters produce thruster exit conditions matching the experimental conditions to within 5%. This has been noted in the same work as a source of uncertainty in comparison with experimental data. The experimental operating condition under consideration here is a high I_{sp}, high voltage configuration, as shown in Table 1. See Table 2 for

the listing of thruster exit simulation parameters used to replicate those operating conditions. It should be noted that the BHT-20K has undergone almost no detailed characterization at the thruster exit and so the determination of appropriate thruster exit conditions is much more difficult than for the Aerojet BPT-4000 thruster studied in 12V previously[2].

The DSMC-PIC boundary conditions pertaining to the Boltzmann model and the detailed-fluid model differ with regard to the ion number density and velocity in order to obtain far-field agreement between the models, as characterized by the axial velocity along the center-line. The flow velocities at the exit are different in order to obtain the far-field agreement and the number densities are adjusted to maintain the desired mass flow rate. This agreement is obtained as shown in Figure 2, in which the thruster exit is located at $z = 3$ m.

Concerning the different types of solid surfaces in 12V, each one is assumed to have a plasma potential of zero, including the baffles, which are electrically grounded. All ions that collide with any wall are neutralized. When particles strike the cryo-pump surfaces, a fraction of them are pumped away. This process is characterized by a sticking coefficient (a value of 0.8 is used for the present study). For the particles scattered back into the flow field from all surfaces, diffuse reflection is assumed which is characterized by the surface temperature.

The facility back-pressure is modeled through static background particles. Each cell contains a few particles with velocities sampled from a zero-centered Maxwellian velocity distribution function. These particles participate in collisions with plume particles and change the velocities of other particles, but their positions and velocities do not change. The back-pressure value for these simulations is set to the value recorded during the experiment, 1.4×10^{-7} torr.

Species	Number Density (1 / m^3)		Axial Velocity (m / s)		Temperature (K)	
	Boltzmann Model	Detailed Model	Boltzmann Model	Detailed Model	Boltzmann Model	Detailed Model
Xe	1.28×10^{18}	1.28×10^{18}	281.3	281.3	750	750
Xe^{+}	1.18×10^{17}	1.39×10^{17}	27792.0	25792.0	23188	23188
Xe^{++}	2.96×10^{16}	3.42×10^{16}	39304.0	36475.0	23188	23188

Table 2: DSMC-PIC input parameters at the thruster exit

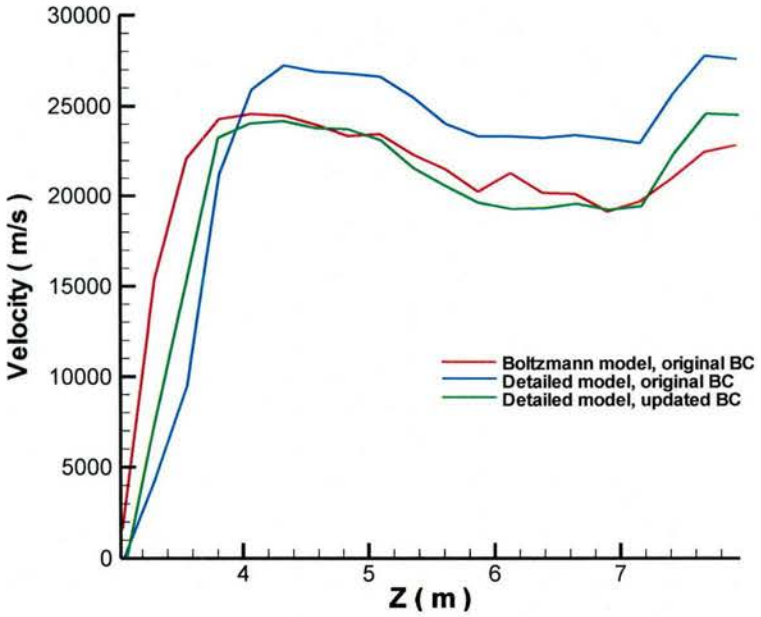

Figure 2: Profiles of Xe^+ axial velocity along the plume centerline

The boundary conditions for the detailed-fluid model must be determined in order to solve Eqs. (5) – (7) above. Since each equation is Laplace-like, each one requires either a Dirichlet (direct) value specified, or a von Neumann (gradient) value specified. The potential, ϕ, the electron temperature, T_e, and the quantity $n_e v_e$ are specified as either direct or gradient at each boundary in the simulation. The value to which each is set is specified in Table 3. Each boundary condition is direct except for the following: 1) each boundary condition for the axis of symmetry is a gradient-type condition, and 2) the wall of the thruster has a gradient-type condition for the electron temperature. Due to the grounding of all the surfaces in the chamber, the plasma potential condition is direct and set to zero for the chamber walls and set to reference values for the thruster exit plane and cathode. The electron temperature is set to nominal values based on previous work and numerical stability. The boundary conditions for $n_e v_e$ are determined using conservation of current as follows:

$$I_d = I_e + I_i \tag{8}$$

$$I_i = j_i * A_{TE} \tag{9}$$

$$j_{d,cathode} = \frac{I_d}{A_{cathode}} \tag{10}$$

where (8) and (9) are used to compute current density at the thruster exit and (10) computes current density at the cathode, from which $n_e v_e$ is found by dividing by the elementary charge e. The sign convention results from electrons flowing out of the cathode, towards the anode. Therefore, the electron velocity stream function must be positive at the cathode and negative at the thruster exit.

Boundary Condition Variable	Thruster		Cathode	Symmetry-line (all gradient-type)	Chamber Walls
	Exit Plane	Body			
$\frac{\partial \Psi}{\partial n}(n_e v_e)$	-1.79×10^{21} $m^{-2}\ s^{-1}$	0	7.32×10^{22} $m^{-2}\ s^{-1}$	0	0
ϕ	50 V	0 V	5 V	0 V m^{-1}	0 V
T_e	10 eV	0 eV m^{-1} (gradient)	2 eV	0 eV m^{-1}	1 eV

Table 3: Detailed fluid-electron boundary conditions

D. Virtual Probe Modeling

A virtual diagnostics algorithm is implemented in order to compare current density predictions to measured data. The virtual probe is analogous to a Faraday cup probe, whereby ions crossing the virtual probe surface are counted. This flux is then converted to current density.

Once the number of ions that pass through the virtual probe face over the course of the simulation is ascertained, this can be converted to a current through the following formula:

$$I = \frac{\sum_k q_k}{t_s} \tag{11}$$

where I is the calculated ion current, q_k is the charge of particle k, and t_s is the total sampling time. Once the current is computed, it is divided by the area of the virtual probe collecting surface to calculate a current density. This allows for a direct comparison to experimental results while still employing an axisymmetric domain. This method is versatile in that it can account for a variety of probe locations and orientations, as well as probe operating parameters such as potential biasing, without affecting the flow-field solution.

Preliminary assessment of the algorithm is performed for a virtual probe with no potential bias, aligned perpendicular to the thruster's acceleration channel at a location 10 cm downstream of the thruster exit plane. Here, the current density can be effectively approximated with the following macroscopic formula:

$$j = \sum_i (n\ u\ q)_i \tag{12}$$

where u is the average axial velocity component of the ions, q_i is the elementary charge of the ion, and n is the local number density of ions. The radial component of the ion velocity can be neglected since it is much smaller than the axial component. The approximated current density using Eq. (12) agrees with the prediction using the virtual probe to within 1.2%.

1.4 Plume Simulation Results

The simulations presented use a total of 250,000 particles at steady state over a domain of 1853 triangular cells. The simulation runs for 800,000 time-steps to reach a steady state and then for another 500,000 time-steps to sample macroscopic data. The time-step size is 2×10^{-6} seconds, resulting in a total sampling time of 1 second. Cases are run at divergence angles of 10°, 20°, and 30°.

A. Flowfield Comparisons

Shown below in Figures 3-8 are field data resulting from the simulations described above. Qualitative effects of divergence angle are observable on each figure, with 10° and 30° cases shown side by side. The difference in current density predictions can be seen in Figures 3 and 5. Note that the current density computed with the conductivity model is not included here due to its similarity with the current density computed by the isothermal model. The effect of using the detailed model is shown to distribute the current density throughout a greater part of the domain when compared to the Boltzmann model. This effect is due to the mathematical nature of the Boltzmann model in that it restricts the dynamic range of the potential. This can be seen directly through the plasma potential (Figures 4, 6, 8), where the Boltzmann model restricts the dynamic range in potential to around 25 V, whereas the detailed models allow for variation of around 50 V. Finally, Figure 7 shows the qualitative difference between the Boltzmann/isothermal models and the conductivity model: the electron temperature is held at a constant 2 eV in the former models and solved for directly in the latter model. This effect can be seen in comparing Figures 6 and 8: the conductivity model predicts even sharper gradients in the plasma potential than the isothermal model.

The effect of divergence angle choice can be observed most explicitly in the Boltzmann model results, and, to a lesser degree, in the results of the detailed models. A smaller value of divergence angle results in a more beam-like plume. This behavior, seen in Figures 3 and 5, indicates the predicted current densities are highly dependent upon the choice of divergence angle. Since divergence angle is strictly a numerical feature not known for the BHT-20K, analyzing a range of angles allows us to fine-tune the results.

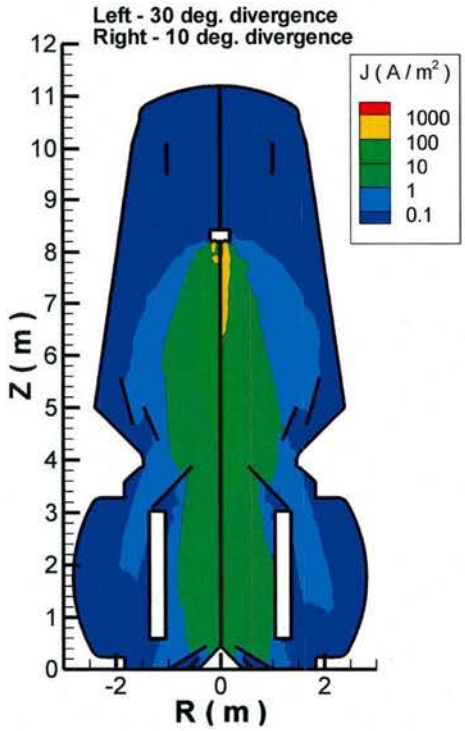

Figure 3: Current density using the Boltzmann fluid-electron model

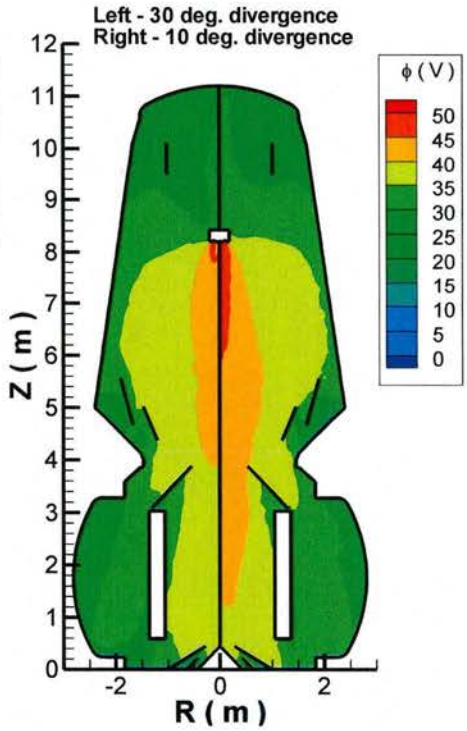

Figure 4: Plasma potential using the Boltzmann fluid-electron model

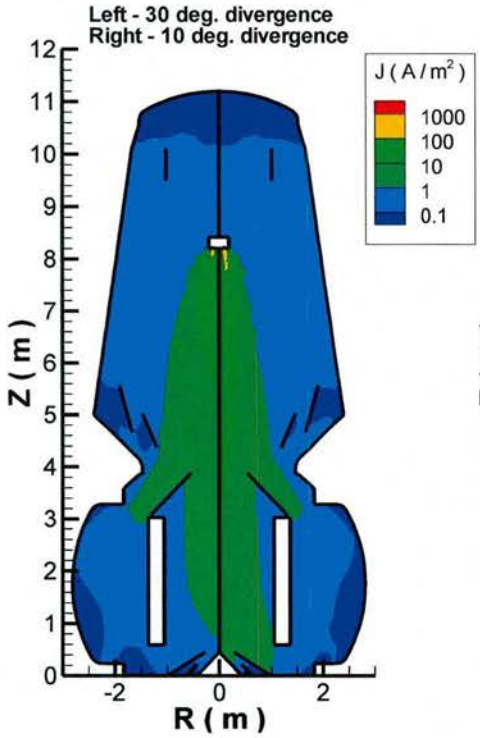

Figure 5: Current density using the isothermal detailed fluid-electron model

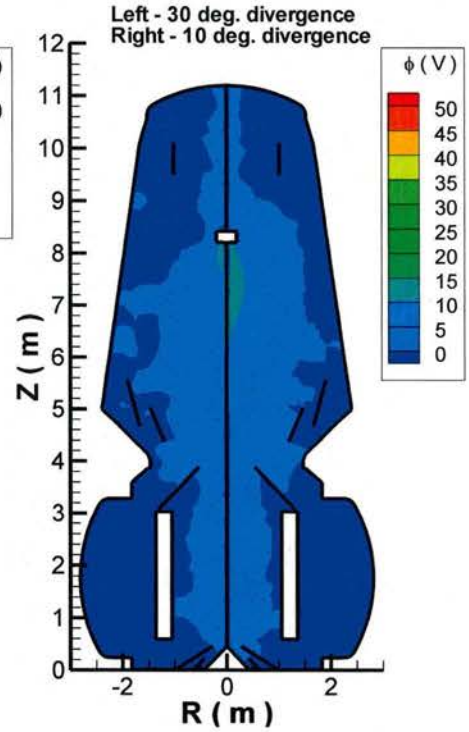

Figure 6: Plasma potential using the isothermal detailed fluid-electron model

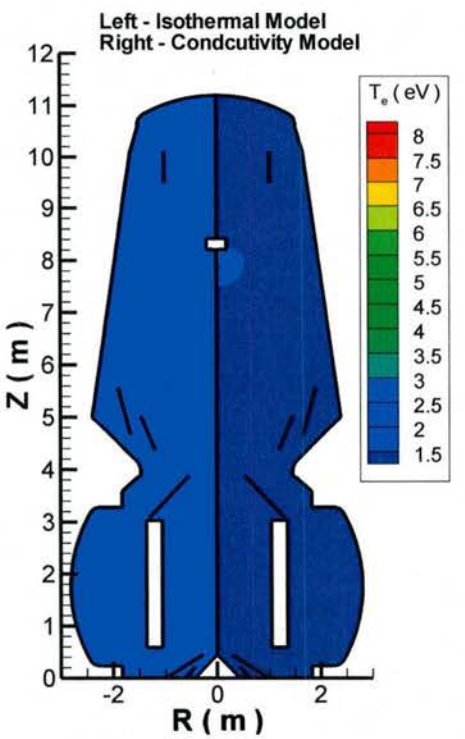

Figure 7: Electron temperature comparisons - conductivity and Boltzmann/isothermal Models

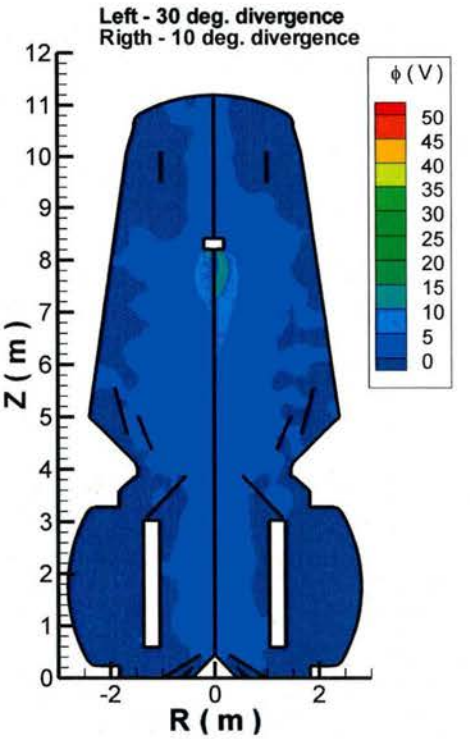

Figure 8: Plasma potential using the conductivity detailed fluid-electron model

B. Experimental Comparisons

Shown below in Figures 9-11 are comparisons between experimental measurements and various simulations. Measured data are reported in Ref. 13 and data acquisition methods are described in Ref. 8 corresponding to the experiments performed in 12V for the Busek BHT-20K Hall thruster at the operating condition under consideration here. Model assessment is performed through comparison with data measured by a set of Faraday cup probes whose locations are shown in Figure 1. Note that two probes are used with two different thruster locations, resulting in four points of experimental measurements, i.e. probes 1 & 2 and 1' & 2'. A third probe was present upstream of probes 1 and 2 but not shown here due to its shorting out at the beginning of the test. General trends seen in Figures 9-11 capture the tendencies observed in experimental measurements; note that discrepancies are tabulated in Table 4 for the 30° divergence angle case using the detailed models only: these models provide the closest comparison when considering the discrepancies as a percent difference between experimental measurements and computational predictions.

The error bars shown are based on probe shielding interference. Probe 1 was shielded by the shorted probe not shown, whereas probe 2 was shielded by both the shorted probe and probe 1. Assuming a maximum shielding based on geometry, the shorted probe shields a maximum of 14% of the ion current for probe 1, while the shorted probe and probe 1 shield a maximum of 37% of the ion current for probe 2.

The two prediction methods utilized are the virtual probe algorithm described above, and evaluation based on the macroscopic properties of the plasma. The macroscopic properties are determined by taking averages of particles within a cell, whereas the virtual probes are implemented only at the experimental measurement locations; as such, the virtual probe predictions are presented below as discrete points. The differences between the macroscopic model and the virtual probe will be discussed below. The virtual probe data are color coded to the fluid-electron model utilized for that case.

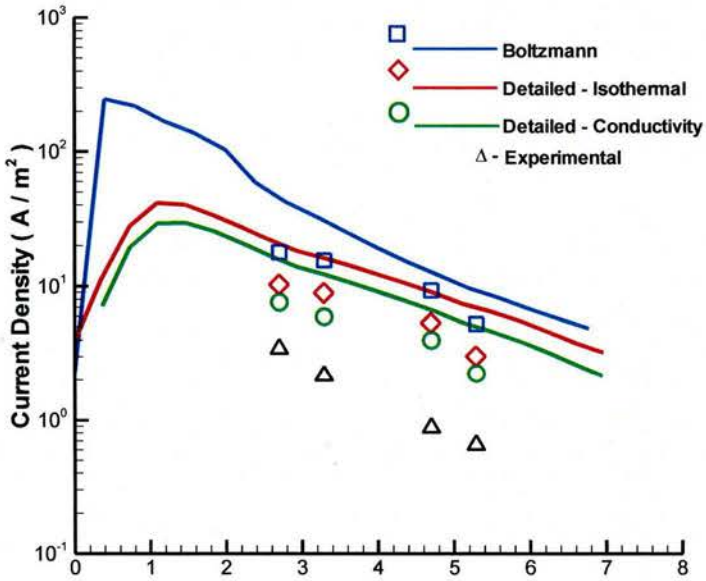

Figure 9: Current density comparisons, 10° divergence angle

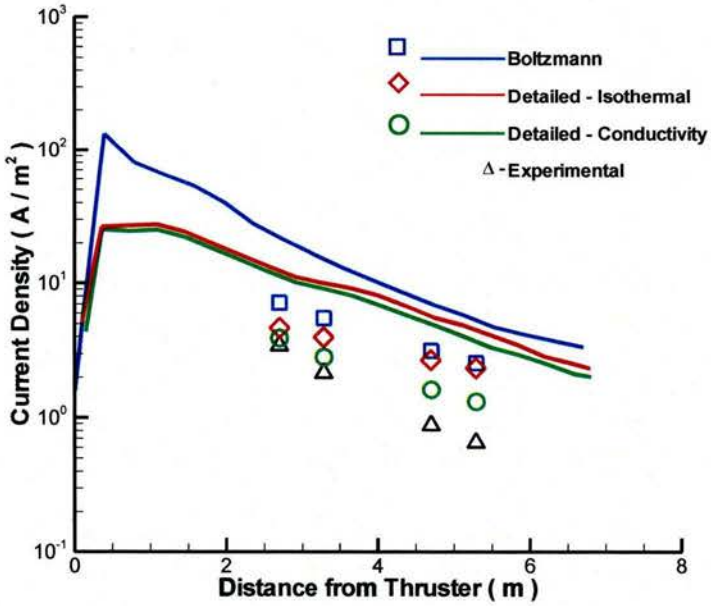

Figure 10: Current density comparisons, 20° divergence angle

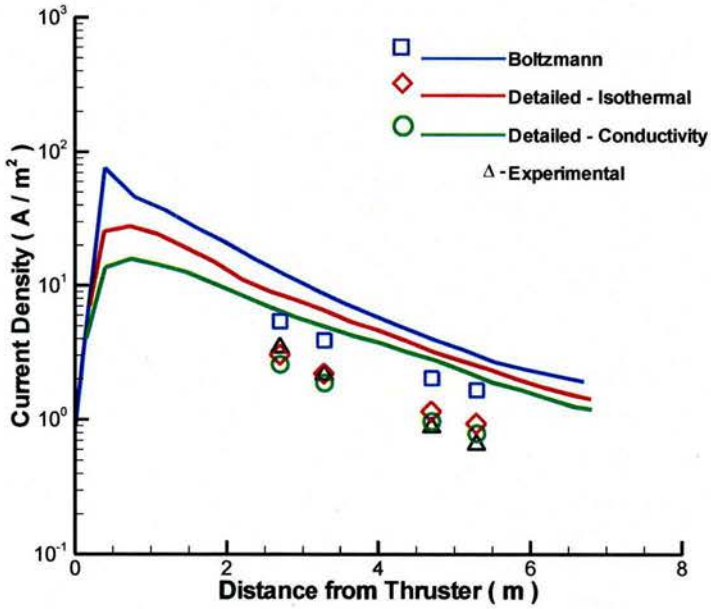

Figure 11: Current density comparisons, 30° divergence angle

	Probe 1	Probe 2	Probe 1'	Probe 2'
Experimental Measurement	$3.45\ \frac{A}{m^2}$	$2.16\ \frac{A}{m^2}$	$0.88\ \frac{A}{m^2}$	$0.66\ \frac{A}{m^2}$
Isothermal	$3.00\ \frac{A}{m^2}$	$2.17\ \frac{A}{m^2}$	$1.13\ \frac{A}{m^2}$	$0.92\ \frac{A}{m^2}$
% Difference Isothermal	-13.04%	0.47%	28.34%	40.10%
Conductivity	$2.55\ \frac{A}{m^2}$	$1.84\ \frac{A}{m^2}$	$0.96\ \frac{A}{m^2}$	$0.78\ \frac{A}{m^2}$
% Difference Conductivity	-26.09%	-14.59%	9.09%	19.08%

Table 4: Tabulated current densities--30° divergence cases

When comparing the predictions to the experimental measurements, agreement depends highly upon model choice and divergence angle. The Boltzmann model virtual probe—10° divergence angle case results in a prediction which only captures qualitative trends in the data, over-predicting measured current density by almost a factor of 10, whereas using either of the detailed models for a 30° divergence angle results in discrepancies of 0.48-40.1%. Most of these discrepancies fall within the uncertainty shown for probe interference.

C. Comparing the Virtual Probe and Maxwellian Models

The significant difference between the predicted current densities using the macroscopic assumption or the virtual probe model, shown in Figs. 9-11, can be explained by analyzing the velocity distributions that each model predicts. The Maxwellian velocity distribution function (VDF) in the axial direction is[14]:

$$f_M(C_1)\,dC_1 = \left(\frac{m}{2\pi kT}\right)^{\frac{1}{2}} exp\left(\frac{-m}{2kT}C_1^2\right) dC_1 \tag{13}$$

The VDF predicted by the virtual probe model is determined by computing a histogram based on the velocities of the recorded particles passing through the probe face. A current distribution function (CDF, *G*) is also computed for a closer representation of the difference in models. The CDF assuming a Maxwellian VDF is computed by Eq. (14). The CDF is computed for the virtual probe using Eq. (15). Shown below in Figures 12 and 13 are the VDF and CDF predicted by each model. By integrating the CDF, the predicted current density is obtained, therefore the total area under each CDF curve represents the current density predicted for each method. A visual comparison of each VDF shows that the velocity distribution corresponding to the ions crossing the virtual probe plane is non-Maxwellian: the beam ions are tightly centered around 29 km/s, with a small group of CEX ions centered at 4 km/s. The corresponding CDF for each method further exhibits the inaccuracy of the Maxwellian assumption at the probe locations: the

integrated current density based on a Maxwellian VDF is much greater than the integrated current density based on the virtual probe. Therefore, a VDF based on the equilibrium assumption is inappropriate. Since the virtual probe is based on discrete particle detection, it captures non-equilibrium effects directly. The result is a current density prediction that falls within the uncertainty associated with the experimental set-up.

$$G_M(C_1) = n_{ions}\, C_{1,i}\, f_M(C_1)\, dC_1 \tag{14}$$

$$G_{VP}(C_1) = \frac{W_{ref} N_{VF}}{A_{VF}\, t_s} f_{VP}(C_1)\, dC_1 \tag{15}$$

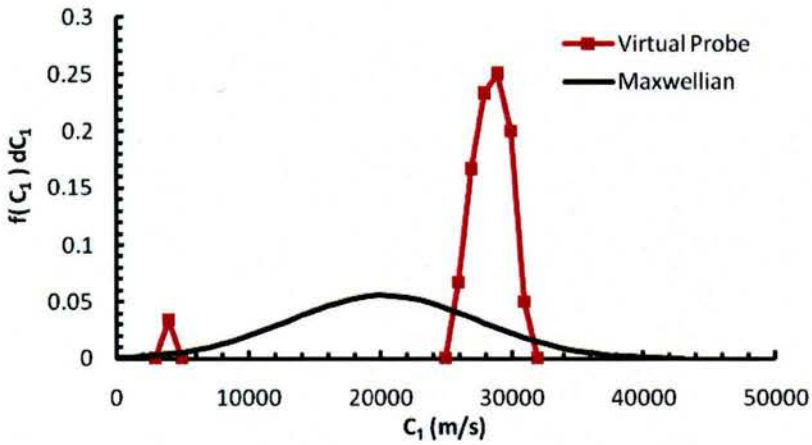

Figure 12: Maxwellian and virtual probe velocity distribution functions at probe 1, divergence angle of 10°, conductivity model case

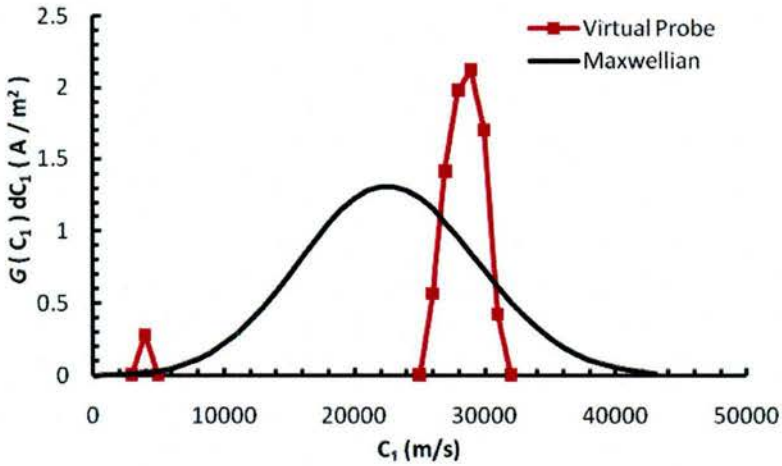

Figure 13: Maxwellian and virtual probe current distribution functions at probe 1, divergence angle of 10°, conductivity model case

1.5 Conclusions

A general purpose, hybrid DSMC-PIC code has been enhanced with a new simulation tool for predicting current densities and a new fluid-electron model which enhances physical modeling fidelity. The new virtual probe model provides enhanced accuracy in comparison to experimental measurements and is flexible enough to provide predictions at locations that were previously lacking instrumentation. This new level of modeling has increased the understanding of the test case under consideration. The inclusion of more robust fluid-electron models alleviated restrictions that were noted in previous work[3] and provided higher correlation with experiment. The result of these new modeling applications showed excellent agreement to experimental measurements, improving prediction capabilities from merely qualitative and deviations from experimental data as large as a factor of 10, to predictions which fall within uncertainties of the measurements.

Further refinement of thruster exit plane boundary conditions and augmentation of the virtual probe model to account for probe operating parameters, such as bias voltage, are areas of future study to better understand the physical situation in the plume. Other areas of study include refinement of the detailed fluid-electron model in order to incorporate all the source terms associated with Eq. (7) while maintaining numerical stability. Specifically, the Joule heating term could play an important role in capturing higher order effects.

References

[1]Boyd, I.D., "Review of Hall Thruster Plume Modeling," *Journal of Spacecraft and Rockets,* Vol. 38, No. 3, 2001, pp. 381-387.

[2]Boyd, I.D., Sun, Q., Cai, C., and Tatum, K. E., "Particle Simulation of Hall Thruster Plumes in the 12V Vacuum Chamber," IEPC-2005-138, 29th International Electric Propulsion Conference, October-November, 2005.

[3]Huismann, T., Boyd, I.D., "Simulation of Hall Thruster Plumes in a Vacuum Chamber Using a Hybrid Method," AIAA-2008-5103, 44th AIAA/ASME/SAE/ASEE Joint Propulsion Conference, Hartford, CT, July 21-23, 2008.

[4]Bird, G. A., *Molecular Gas Dynamics and the Direct Simulation of Gas Flows*, Clarendon Press, 1994.

[5]Birdsall, C. K., and Langdon, A. B., *Plasma Physics via Computer Simulation*, Adam Hilger, U.K., 1991.

[6]Boyd, I.D., and Yim, J.T., "Modeling of the Near Field Plume of a Hall Thruster," Journal of Applied Physics, Vol. 95, No. 9, 2004, pp. 4575-4584.

[7]Pruitt, D., Dawbarn, A., Bauer, M., *et al.*, "Development of a Novel Electric Propulsion Test and Evaluation Capability at AEDC," AIAA -002-4338, 38th AIAA/ASME/SAE/ASEE Joint Propulsion Conference, Indianapolis, IN, July 7-10, 2002.

[8]Raitses, Y., Moeller, T., and Szabo, J., "AEDC Plume Measurements using bi-directional ion flux probes," IEPC-2007-334, 30th International Electric Propulsion Conference, Florence, Italy, September 17-20, 2007.

[9]Miller, J. S., Pullins, S. H., Levandier, D. J., Chiu, Y., and Dressler, R. A., "Xenon Charge Exchange Cross Sections for Electrostatic Thruster Models," *Journal of Applied Physics*, Vol. 91, No. 3, 2002, pp. 984-991.

[10]Chen, F.F., *Introduction to Plasma Physics and Controlled Fusion*, Vol. 1: Plasma Physics, Plenum Press, 1984.

[11]Cai, C., *Theoretical and Numerical Studies of Plume Flows in Vacuum Chambers*, PhD Thesis, University of Michigan, 2005.

[12]Choi, Y., Keidar, M., Boyd, I.D., "Particle Simulation of Plume Flows from an Anode-layer Hall Thruster," *Journal of Propulsion and Power*, Vol. 24, No. 3, 2008, pp. 554-561.

[13]Polzin, K.A., Szabo, J., Byrne, L., Raitses, Y., Dawbarn, A., Tatum, K.E., Crider, D., Brown, M., Bynum, K., Crews, D., Moeller, T., and Boyd, I.D., "Demonstration of High Power Plasma Propulsion Test Capabilities at Arnold Engineering Development Center," 54th Joint Army-Navy-NASA-Air Force (JANNAF) Propulsion Meeting (JPM) / 5th Modeling & Simulation Subcommittee (MSS) / 3rd Liquid Propulsion Subcommittee (LPS) / 2nd Spacecraft Propulsion Subcommittee (SPS) Joint Meeting, Denver, CO, May 14-17, 2007. (ITAR Restricted)

[14]Vincenti, W. G., and Kruger, Jr., C.H., *Introduction to Physical Gas Dynamics*, Krieger Publishing Company, 1965.

Part 2-- Spectral analysis of simulated Hall thruster discharge current oscillations

Nomenclature

I_d = discharge current
F_{th} = force due to thrust
f = frequency
Δt = base (ion) time step
Δt_e = electron subcycle time step
m_a = mass of species a
n_a = number density of species a
q = elementary charge
ν_a = collision frequency for phenomenon a
μ_{ez} = axial, cross-field electron mobility
α = location-based scaling coefficient for electron mobility modeling
ω_a = plasma frequency of species a
Z = charge number
B_i = magnetic field, i component

2.1 Introduction

Hall thrusters are known to generate oscillation modes as a result of physical processes, some of which are known and others which are still being observed and studied {Choueiri, 2001}, making time-varying modeling an important research topic. For the past decade, the Hall thruster model HPHALL has been the focus of much research and development. HPHALL performs an axisymmetric simulation of the plasma within the thruster discharge chamber and near-field plume which employs both fluid and particle-in-cell (PIC) numerical methods {Fife, 1998}. The code has been found to be potentially effective in creating either time-averaged outputs of performance data which could be used, for example, as source terms into an erosion mode {Hofer et al., 2007}, or to observe and analyze the time-varying nature of the detailed evolution of the internal plasma of a Hall thruster at small timescales {Parra et al., 2006}. However, it seems that the time-varying results have undergone less scrutiny due to the fact that while time-averaged results are tunable for accurate steady-state comparisons to experiment, time-varying observations can be plagued with inconsistencies. It is this time-varying nature and subsequent phenomena of time-varying operation which is the focus of this report.

This report provides a brief introduction to the Hall thruster under consideration and the simulation code. The methods of comparison for the present work are outlined whereby simulated results of both performance and spectral analyses are compared to experimental results for assessment purposes. Assessment of the code's ability to replicate accurate performance output is shown to be successful for time-averaged data for the Hall thruster's operating conditions of interest. However, some of the numerical parameters used in the simulation of these operating conditions are shown to have adverse effects on the response of physical models. Varying responses due to physical models are then shown to have an effect on time-varying characteristics of the performance output. The results and disparities of this assessment demonstrate the consequent need for a more detailed look at numerical schemes of the physical

models as well as the numerical parameters employed. Steps are taken to vary simulation particle population, time step, and the length scales of certain physical models in order to study the way in which time-varying data is affected.

2.2 Technical Approach

A. Hall thruster and Experiments

The experiments used for the comparison purposes of this study were performed by Reid using a 6 kW laboratory model Hall thruster {Reid, 2009}. Experiments were performed in the Large Vacuum Test Facility (LVTF), a 6 m diameter by 9 m long cylindrical, stainless steel chamber with seven cryopumps, at the University of Michigan's Plasmadynamics and Electric Propulsion Laboratory (PEPL). The thruster was operated on a 100 kW power supply using a separate 1 kHz RC discharge filter for protection. Commercially available power supplies were used to power the cathode heater, cathode keeper, and magnet circuitry. Research grade xenon propellant (99.999% pure) was used for cathode and anode supply.

In order to gather time-averaged discharge current data, a calibrated current shunt and multimeter were used in correlation with the main discharge power supply read-out. Time-varying discharge current data was gathered using a commercially available, high-speed current shunt rated for 100 kHz and placed on the cathode return line in between the thruster and RC filter.

B. Numerical Model

The computer code HPHALL performs an axisymmetric simulation which is commonly referred to as ``hybrid-PIC", utilizing fluid approximation equations in the treatment of electrons and a particle-in-cell (PIC) method in the treatment of heavy species, namely singly- and doubly-charged xenon ions and atoms. The electron equations are solved at a smaller time step, called the electron subcycle, in order to simulate how the speed of electrons is much faster than that of a heavy species. This allows for electron fluid equations to be fully solved and settled in between xenon particle updates. Hybrid fluid-particle methods have been shown to be successful in Hall thruster plume studies {Boyd, 2001} and are computationally cheaper than fully kinetic methods {Szabo, 2001}. The code was originally created by Fife and Martinez-Sanchez {Fife, 1998} and then later advanced by Gamero-Castano and Katz to include such upgrades as a more detailed sheath model and a sputtering yield algorithm for the use as an erosion model {Gamero et al., 2005}. Parra et al. also made certain advances by way of improving such algorithms as heavy particle modeling, electron mobility modeling, plasma weighting, and ionization models, among others {Parra et al., 2006a, 2006b}. Further development and corrections were performed by Hofer et al. on the heavy particle modeling, erosion sub-model, and electron mobility physics, continuing the development of the code to the present version. {Hofer et al., 2006, Hofer et al., 2007a, 2007b, Hofer et al., 2008} Through this past work, the code has a favorable history of presenting good agreement with macroscopic properties, such as discharge current and thrust, as well as local properties, such as plasma density, plasma potential, and electron temperature. An example of this time-averaged output of the code can be seen in Figure 1 which is a representation of electron number density at optimal operating conditions, detailed in the next

section. For this type of two-dimensional contour plot, the anode is located on the left side and the near-field plume is located on the right side of the domain.

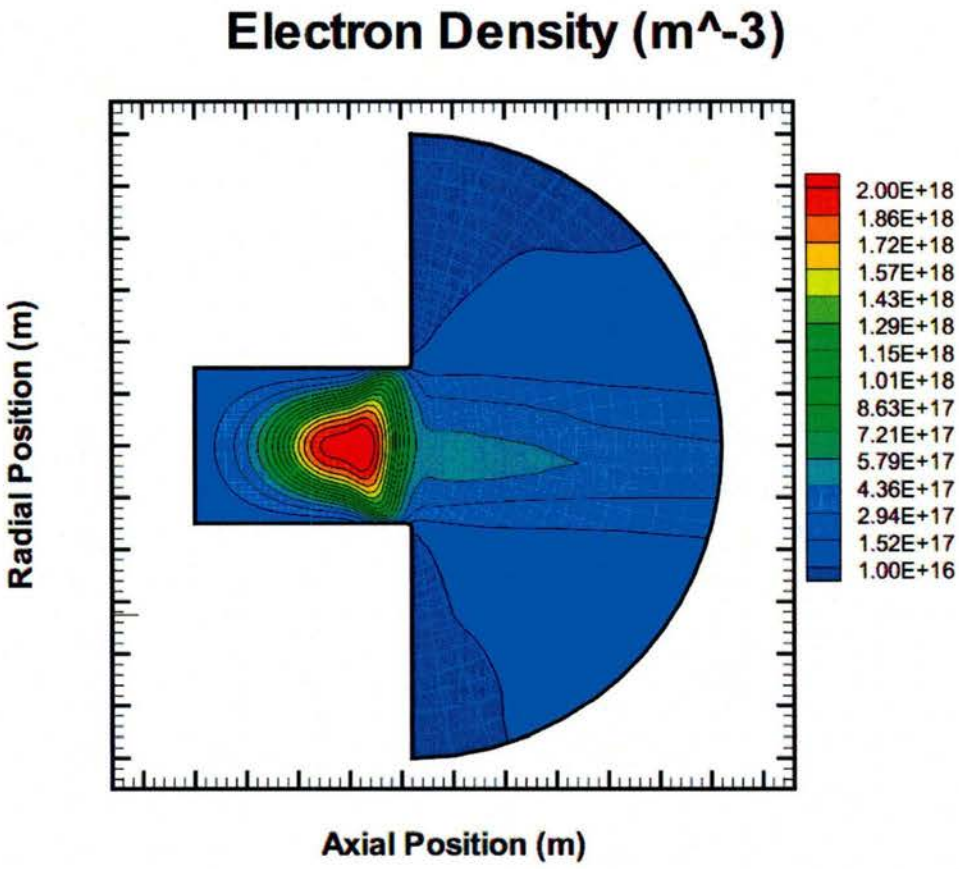

Figure 1: Axisymmetric, time-averaged electron number density contours

3.3 Results

A. Code Assessment

In order to assess the code using experimental results, simulations are performed at several different, physical operating conditions which are nominal to the thruster's operation and explained in detail later. Simulations are performed by injecting neutral xenon into the domain, with plasma physics turned off, for approximately 1 ms of simulated time followed by approximately 4 ms of simulated time where the plasma physics are turned on. For example, when operating at the time step Δt = 5e-8 s, 20,000 iterations of neutral injection are followed by 80,000 iterations of plasma simulation. At these operating conditions, and using approximately 300,000 particles, this simulation requires about 12 hours of computer run time. All comparisons are performed with electron subcycles of either 0.01 Δt or 0.001 Δt which have little effect on either the time-averaged or time-varying solutions of the simulation. The electron subcycle is discussed further in the time step study section.

Flowrate	I_d (A) Experiment	I_d (A) HPHALL	% Diff.	F_{th} (N) Experiment	F_{th} (N) HPHALL	% Diff.
10 $^{mg}/_{sec}$	9.06	8.82	2.6	0.185	0.175	5.4
20 $^{mg}/_{sec}$	19.94	19.80	0.7	0.398	0.394	1.0
20 $^{mg}/_{sec}$	19.94	19.88*	0.3	0.398	0.386*	3.0
30 $^{mg}/_{sec}$	33.80	32.14	4.9	0.620	0.599	3.4

Table 1: Hall thruster operating conditions for both experiment and simulation at a discharge voltage of 300 V. * indicates facility background pressure included.

Nominal experimental operating conditions include discharge voltages of 150 V, 300 V, and 600 V at mass flow rates of 10, 20, and 30 mg/s. Simulations are run at all operating conditions but are focused on the optimal operating conditions of 300V, 20 mg/s. Simulated, time-averaged performance data are compared to experimental performance data. The two major comparisons being discharge current, I_d, and thrust, F_{th}, and show that simulated results are very accurate. This comparison of varying flowrate for the optimal discharge voltage of 300 V can be seen in Table 1. Included in Table 1 is the condition of added facility background pressure, an algorithm which injects neutral particles at the simulation boundary. This method brings performance output closer to experimental results and ultimately simulates a more accurate portrayal of the real system. The reason for the best agreement at optimal conditions is because of the internal tuning of electron mobility physics within the simulation which has been pre-set to show the best agreement with these optimal conditions, the conditions that the Hall thruster is designed for and at which it would most likely be operated. This time-averaged comparison shows very good agreement between simulation results and experimental measurement at the operating conditions of interest.

Discharge oscillations from both simulation and experiment are also compared via power spectra. Simulated trends can be seen in the Hall thruster discharge current spectral power analysis found in Figure 2 and show relatively good agreement with experimental data {Reid, 2009}, also found in Figure 2 (using the same color scheme for the purpose of comparison), though the agreement is far from exact. The noisy simulated data has been processed through a basic, one-dimensional smoothing algorithm for the purely observational purposes of comparing relative magnitudes and trends. In terms of absolute values, it is found that the model simulates a much larger magnitude discharge current oscillation than the experimental data. At optimal operating conditions, data from Reid {Reid, 2009} report a standard deviation of the discharge oscillations as approximately 8% of the mean discharge current whereas the simulations show an approximately 8-25% oscillation (depending on time step size and mobility model, as will be shown later), which translates to approximately 25-50% in peak-to-peak terms. The familiar breathing mode oscillation appears in the range of 10-30 kHz in both spectra. A higher frequency mode is also clearly present at around 70-100 kHz although its source is not clear. While the fact that this mode is seen in both data sets seems like a potentially important finding, it will be shown that the computational result is sensitive to physical modeling and numerical parameters. These results give a glimpse into the details of such time-varying phenomena which will affect the validity of time-varying comparisons.

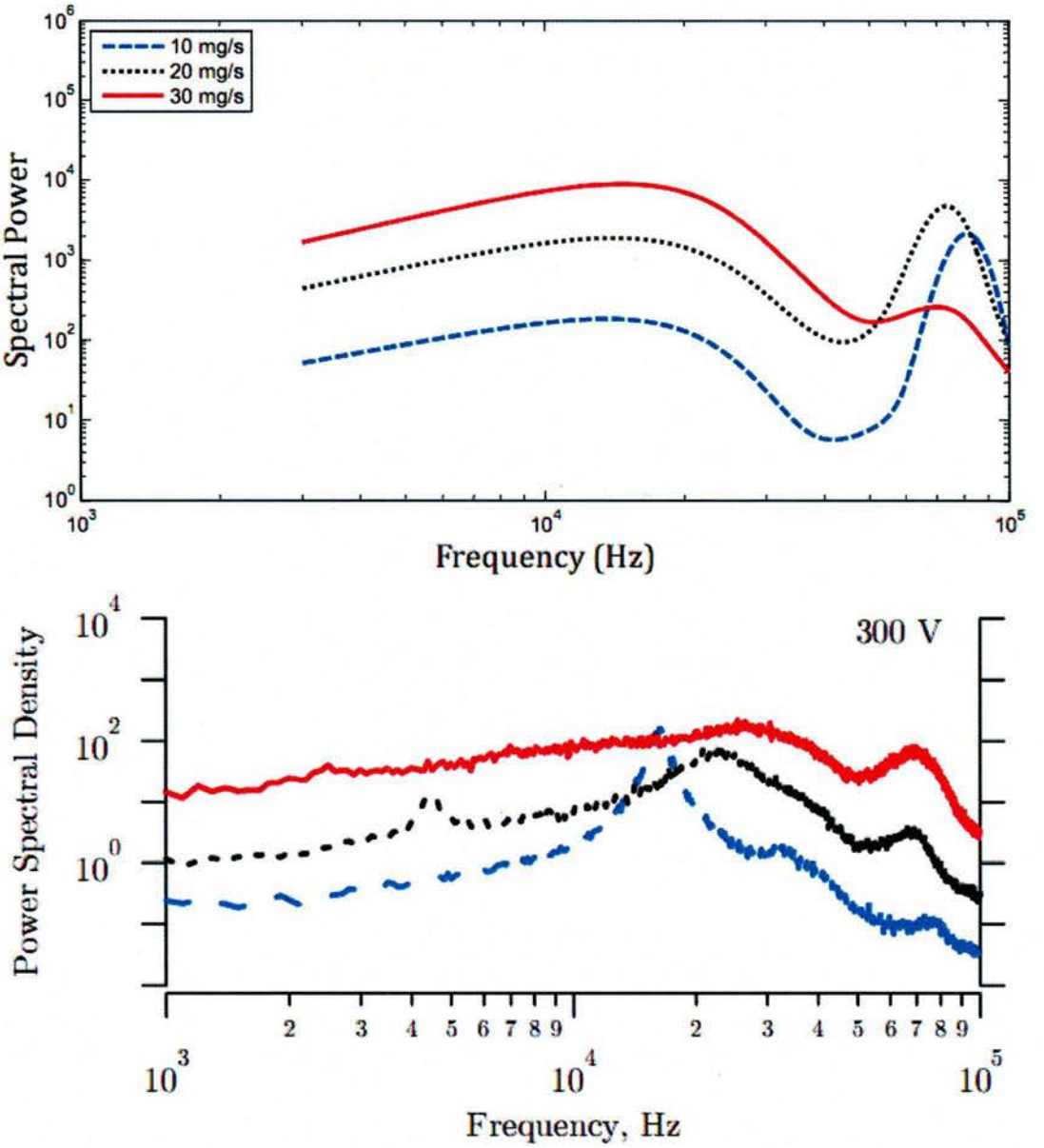

Figure 2: Power spectral density, simulation (top) and experiment (bottom).

B. Effects of Electron Mobility Modeling

The first phenomena which must be discussed are the electron mobility models currently available within HPHALL and their effects on time-varying solutions. Cross-field electron mobility is modeled in the code as {Hofer et al., 2008}:

$$\mu_{ez} \simeq \frac{\nu_e m_e}{qB_r^2}, \tag{1}$$

a measure of the propensity for electrons to cross magnetic field lines axially rather than stay in an azimuthal drift within the discharge channel. The effective electron collision frequency, ν_e, is given by

$$\nu_e = \nu_{ei} + \nu_{en} + \nu_{\text{wall}} + \nu_{\text{bohm}} \tag{2}$$

with ν_{en} as the electron-neutral collision frequency, ν_{ei} as the electron-ion collision frequency, ν_{wall} as the collision frequency of the electrons with the walls, and ν_{bohm} as a collision frequency due to anomalous Bohm diffusion for electrons. The anomalous Bohm diffusion parameter is a user-augmented parameter which holds the purpose of matching simulated, effective collision frequencies with those of experimental measurements. Anomalous Bohm diffusion is modeled in the code as

$$\nu_{\text{bohm}} = \alpha \frac{1}{16} \omega_{ce} \tag{3}$$

where α is an arbitrary parameter adjusted to match experimental results by providing for the necessary location-based cross-field diffusion values. For example, the case for classical Bohm diffusion uses $\alpha = 1$. HPHALL was originally created with a single value for α and then moved to a two-region model, with separate values of α_c and α_p for the channel and the plume, respectively, after it was found that a two-region model shows an improvement in accuracy on similar but different codes {Hagelaar et al., 2003, Koo et al., 2006}. A three-region model was later implemented by Hofer et al. {Hofer et al., 2008} in order to more closely align cross-field mobility to the distribution of the Hall parameter within the channel, separating the parameter into α_c, α_e, and α_p for the channel, acceleration region, and plume, respectively. A visual representation of the three-region mobility model can be seen in Figure 3. The previous, two-region model can also be visualized by combining Regions I and II of Figure 3. As used by Hofer et al. and in order to maintain consistency, in the present study values of $\alpha_c = 0.044$, $\alpha_p = 1$ are used for the two-region model and $\alpha_c = 0.08$, $\alpha_e = 0.016$, $\alpha_p = 10$ are used for the three-region model.

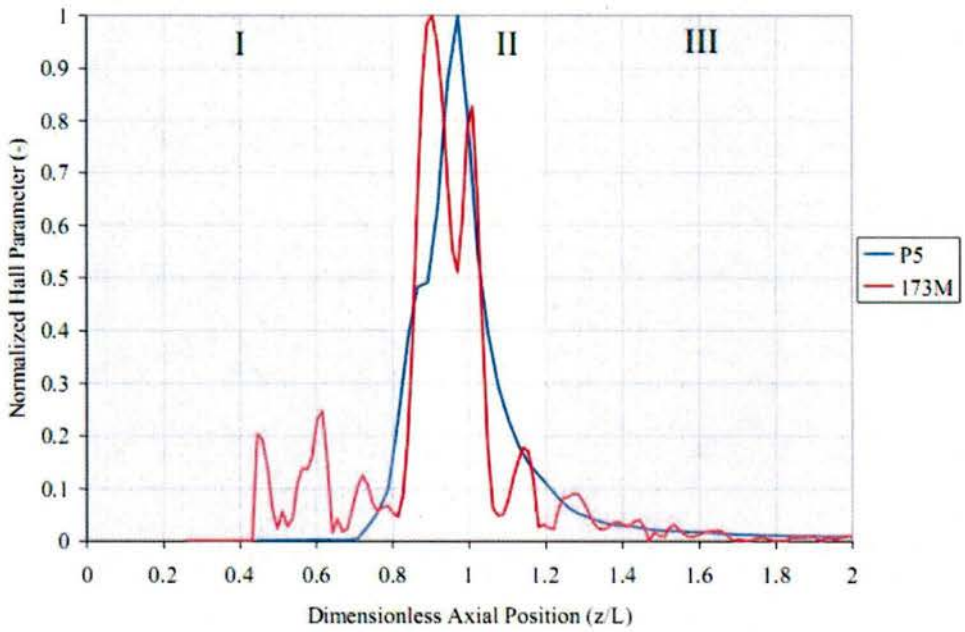

Figure 3: Experimental data of Hall parameter versus axial position along with representation of mobility region.

The simulated discharge current traces of the three-region mobility model produce more easily distinguishable features than the two-region model results, shown in Figure 4 in which the three- and two-region mobility models are compared side by side. The three most profound phenomena found in the three mobility region current traces are the breathing mode oscillation, a higher-frequency mode called the ``three-region artifact'', and the discharge current lag from the beam to the anode. Common to both mobility models are the lag and breathing mode oscillations. In addition, as mentioned earlier, the three-region model predicts a standard deviation in the discharge oscillations of about 8-25\% of the mean discharge current while the two-region model predicts a steady deviation of approximately 8\%. These relative magnitudes can be seen in the side by side comparison. The spectral analyses of two-region and three-region simulations can be found in Figure 5 for four different simulation time steps, showing significant differences in the results produced by the two mobility models. The time steps used in this parametric study are Δt = 5e-9 s, 2.5e-8 s, 5e-8 s, and 10 e-8 s.

A major feature found in the three-region current traces is the high-frequency mode which has a timescale of about 1.5e-5 s, corresponding to a frequency range of about 60-80~kHz which can be identified as the sharp peaks in the spectra of Figure 5. This mode is completely absent in the two-region results. In addition, higher frequency harmonics due to the high-frequency mode are not observed in the larger time step of Δt = 10e-8 s, instead only displaying a single spectral spike. This indicates that the oscillation mechanism occurs at a timescale somewhere in between Δt = 5e-8 s and Δt = 10e-8 s.

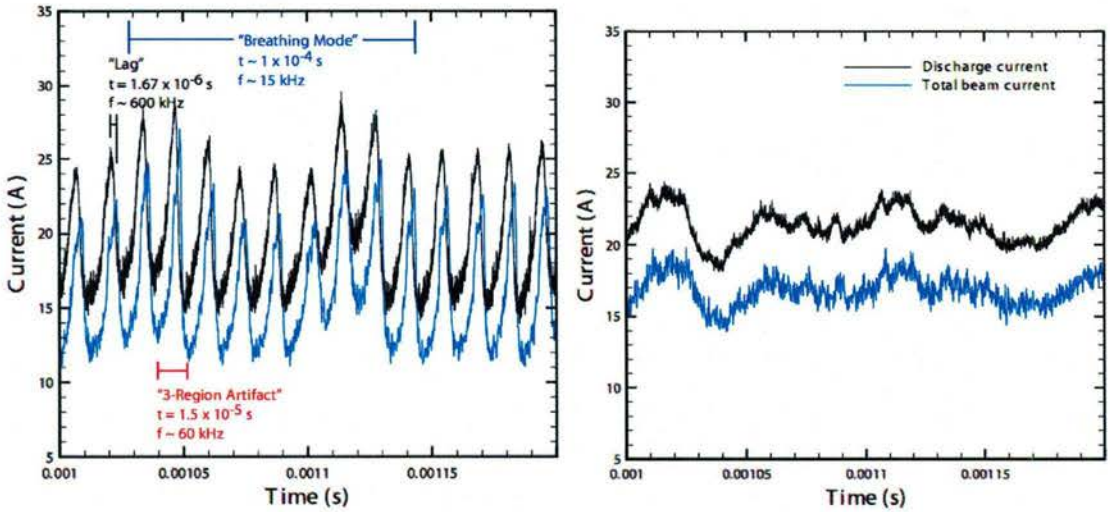

Figure 4: Simulated and beam current profiles using three region (left) and two region (right) models.

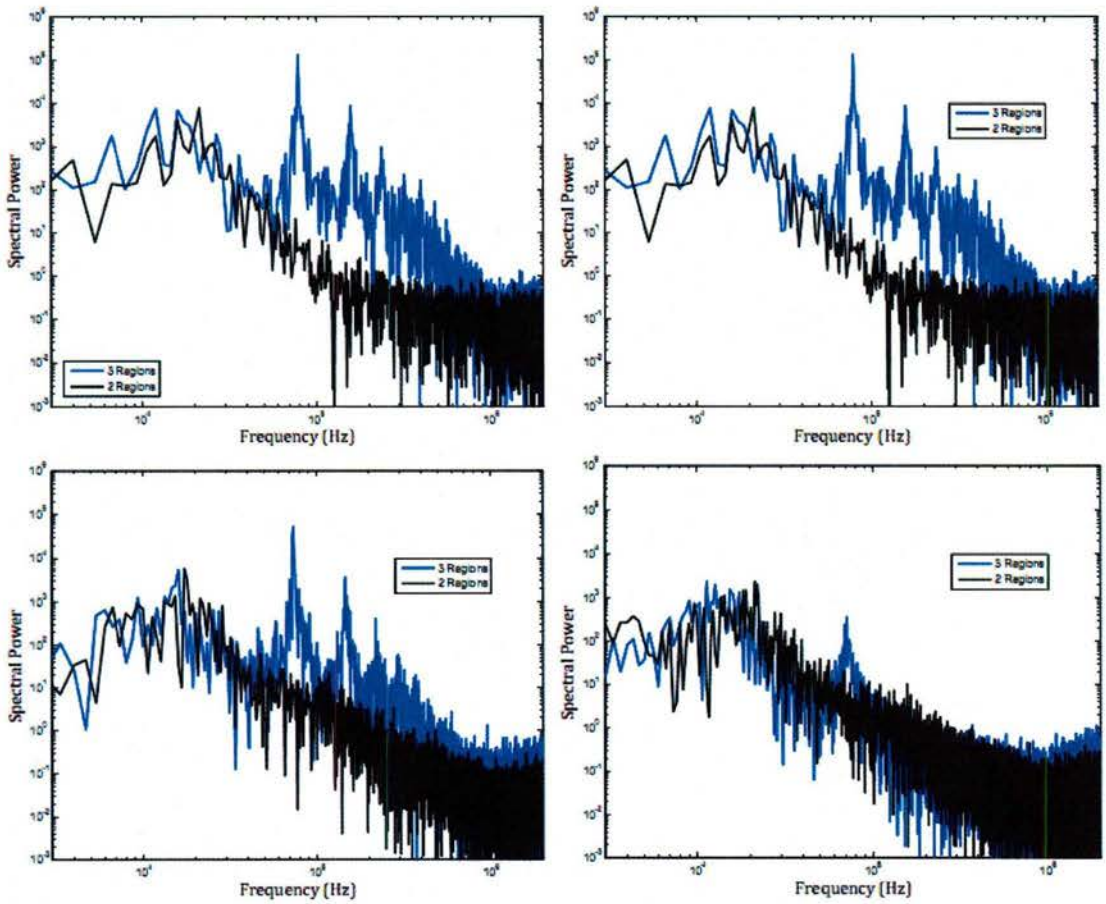

Figure 5: Spectral analysis for two and three region models; Δt = 5e-9 (top left), 2.5e-8 (top right), 5e-8 (bottom left), and 10e-10 (bottom right).

C. Effects of Numerical Parameters

Despite the similarity of the power spectra trends between experiment and simulation for the 6~kW Hall thruster, it is found that certain numerical parameters greatly affect the simulated time-varying solutions (as previously portrayed by Figure 5) while the time-averaged solutions remain relatively unchanged. In addition, these varying results are mobility-model specific. Part of the evaluation process of the code is to study any sensitivity of the solutions to the numerical parameters. Simulation particle population, time step, and the acceleration region (region II) length scale of the mobility model are varied in order to characterize the different time-varying solutions.

Spectral analysis is performed on the discharge current signal at varying particle populations and the results are shown in Figure 6 in which the three-region mobility model is used. The numbers of both neutral and singly-charged xenon are varied and show no change or shift in spectral components at the Hall thruster oscillation modes of interest. Low frequency results cannot be explained but seem to be weakly coupled to particle population. However, it has been observed experimentally and speculated that one source of such low frequency oscillations, often called the ``spoke" mode, is coupled to density nonuniformities and ionization processes {James et al., 1966}. The spoke mode is impossible to capture in HPHALL because the phenomenon is inherently azimuthal while the simulation operates in a radial-axial, axisymmetric manner. At these varying ion and neutral populations, time-averaged results, as well as two- and three-region results, vary by a negligible amount.

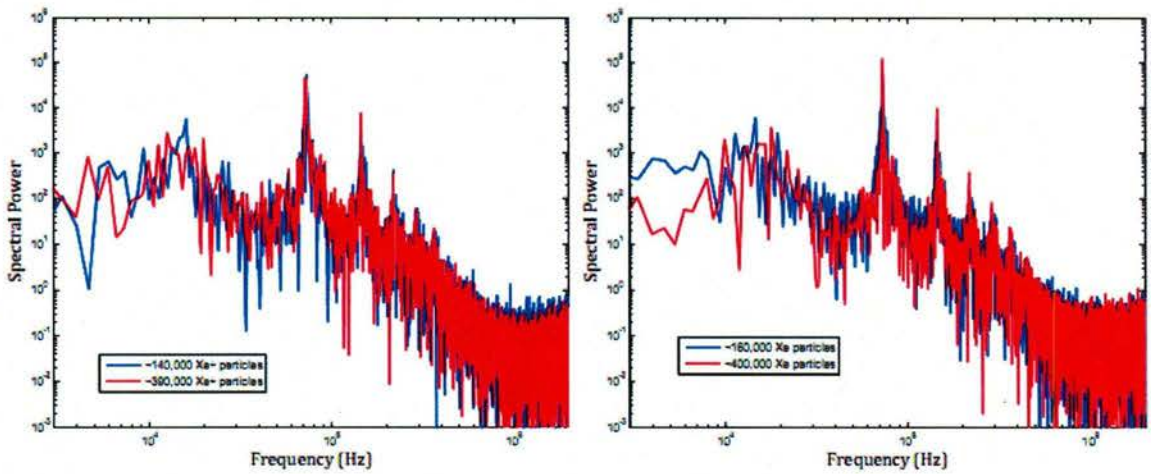

Figure 6: A comparison of power spectra, varying singly charged (left) and neutral (right) particle populations using three region mobility model.

Spectral analysis is also performed on the discharge current signals obtained with different time steps for both two-region and three-region simulations and the results are shown in Figure 7. At these different time steps, time-averaged results show significant changes in discharge current and thrust (see Table 2), one of the first indications of numerical sensitivity in the three-region mobility model. Table 2 also displays the very small difference in time-averaged results for varying electron subcycle. Decreasing time step shows a significant increase in the

magnitude of the discharge current oscillations at higher frequencies when operating with the three-region model. This is not observed in the two-region simulations with the exception of the smallest time step, Δt = 5e-9 s, though the high-frequency mode is still not present. Furthermore, both the two-region and three-region models show similar trends in changing time-averaged data with decreasing time step, the trend in Table 2 showing increasing magnitudes until the smallest time step. Two simulated discharge current oscillations operating with the three-region mobility model and with an order of magnitude difference of simulation time step are shown side-by-side in Figure 8, displaying the magnitude increase and shift. It is also observed that the oscillations around the mean discharge current are not symmetric; the positive oscillations are of higher magnitude than the negative oscillations. The smaller time step simulations result in generally higher magnitude oscillations reaching peak-to-peak values on the order of about 50% the mean discharge current value, as mentioned before.

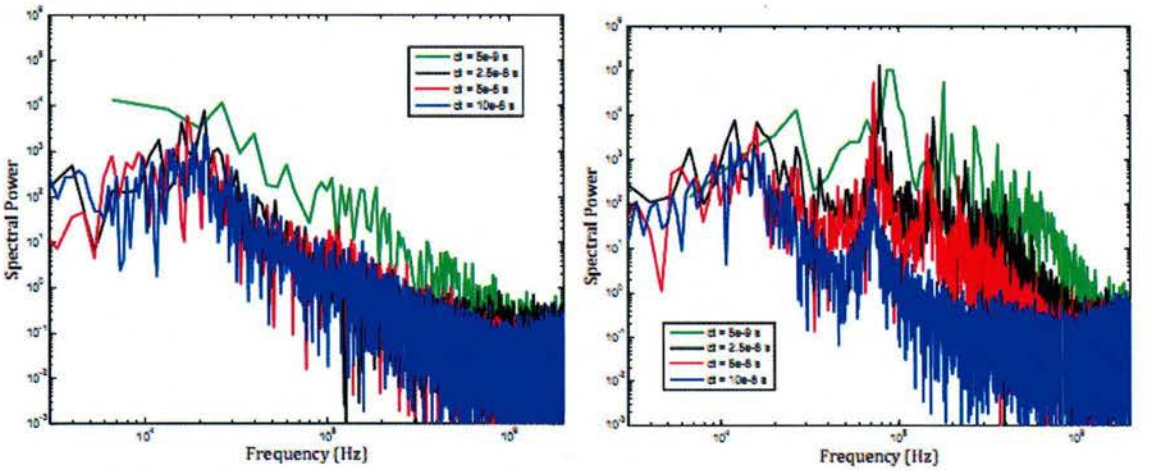

Figure 7: A comparison of power spectra, varying time step using two region (left) and three region (right) models.

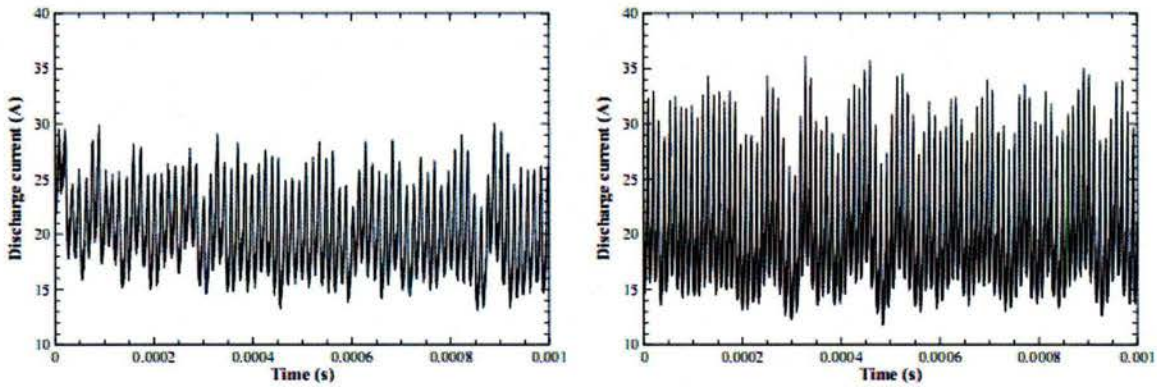

Figure 8: Simulated discharge current, using time steps of 5e-8 (left) and 5e-9 (right) at optimal operating condition.

$\Delta t_e = 0.01\Delta t$			$\Delta t_e = 0.001\Delta t$		
Δt	I_d (A)	F_{th} (N)	Δt	I_d (A)	F_{th} (N)
5×10^{-9} sec	19.72	0.377	5×10^{-9} sec	19.69	0.377
2.5×10^{-8} sec	20.12	0.387	2.5×10^{-8} sec	20.14	0.388
5×10^{-8} sec	19.86	0.389	5×10^{-8} sec	19.98	0.391
10×10^{-8} sec	19.09	0.390	10×10^{-8} sec	19.12	0.390

Table 2: Simulated time averaged performance data for three region model.

In order to verify that the simulation time steps are appropriate, electron and ion frequencies are calculated {Nicholson, 1983} using Equations 4 and 5. These frequencies correspond to ion timescales of approximately 1e-9 s to 5e-7 s, seen in Figure 9, and electron timescales which are approximately 500 times smaller. Despite this difference, it is important to note that at the larger electron subcycle, $\Delta t_e = 0.01\Delta t$, solutions still show little to no disparity.

More than an order of magnitude difference in time scale occurs between the bulk of the discharge within the channel and the near-plume region. These results show that the two smallest time steps, 5e-9 s and 2.5e-8 s, are small enough to capture macroscopic plasma phenomena throughout the whole domain. The 5e-8 sec time step seems small enough yet very close to the timescales within the bulk discharge in the channel. The 10e-8 s time step is too large to resolve the detailed properties of the channel discharge (the bluest contours in Figure 9). This reinforces the previous observation that some of the high-frequency modes present in the spectral analyses of the smaller time steps are missing in the 10e-8 s studies.

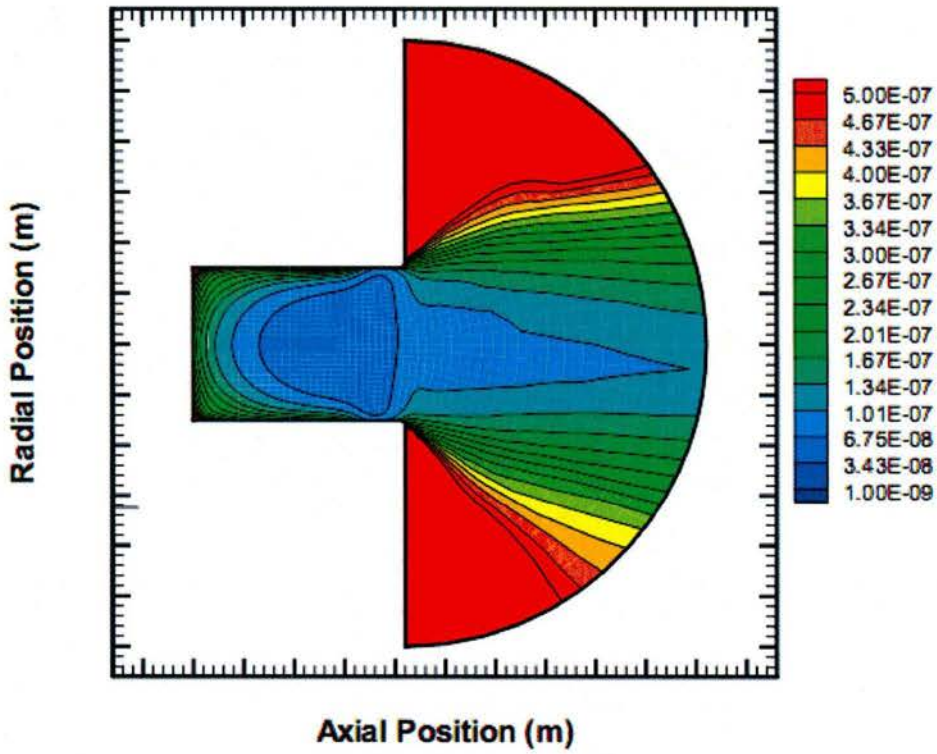

Figure 9: Two dimensional, time averaged contours of ion timescales.

$$\omega_e \equiv \left(\frac{4\pi n_e q^2}{m_e}\right)^{1/2} \tag{4}$$

$$\omega_i \equiv \left(\frac{4\pi n_i Z^2 q^2}{m_i}\right)^{1/2} \tag{5}$$

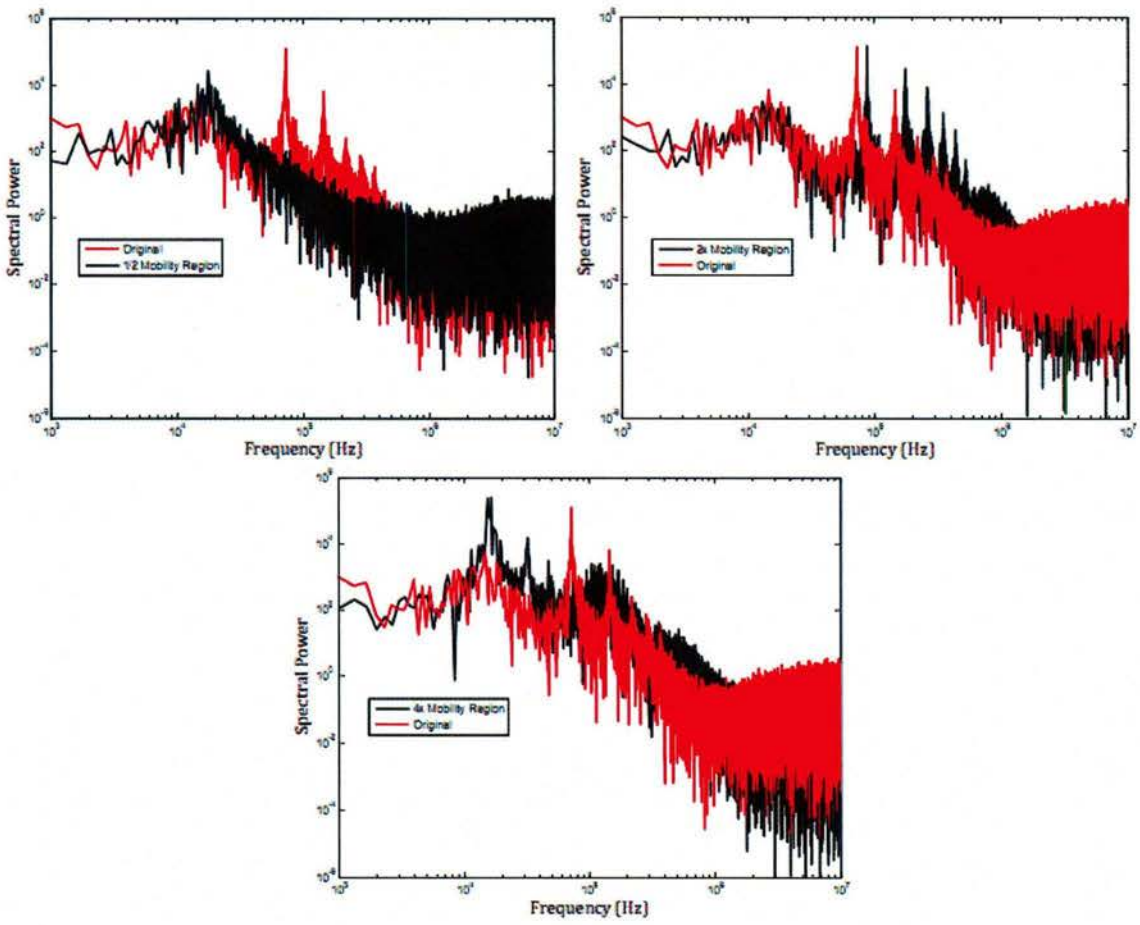

Figure 10: Spectral analyses, three region mobility model, for half (top left), double (top right), and four times (bottom) the original size of region II.

Spectral analysis is also performed on the discharge current signals obtained with different lengths of region II of the three-region simulations and the results are shown in Figure 10. At these different lengths, time-averaged results show significant changes in discharge current and thrust (see Table 3). Firstly, it is important to note that without proper tuning of the mobility coefficient, α, time-averaged data from differing mobility regions will rarely match

well. The purpose of changing mobility region lengths is primarily to observe any response of the high-frequency mode so that further analysis can be made of its physical nature.

Changing the acceleration region to half its original size (top left of Figure 10) results in a loss of the high-frequency mode, possibly because of the inability to resolve the physics introduced in this region. Doubling the size of region II (top right of Figure 10) shifts the high-frequency modes approximately 15 kHz higher. Increasing the size of region II to four times the original length (bottom of Figure 10) creates a sharper spike and resonances at the breathing mode and a broader bump centered at about 100 kHz. The responses of both time-averaged and time-varying data with varying mobility region size shows that the physical nature of the high-frequency mode might very well be associated with the physics captured by sizing the mobility regions to experimentally observed Hall thruster data, as previously portrayed by Figure 3.

Region II Size	I_d (A)	F_{th} (N)
Original	19.98	0.391
Half	22.48	0.404
Double	17.04	0.351
$\times 4$	15.86	0.342

Table 3: Simulated, time averaged performance data for three region model, varying acceleration zones.

2.4 Conclusions

Numerical modeling of a 6kW Hall thruster has been performed using an established hybrid fluid-PIC simulation code. Comparisons of numerical results to measurements of time-averaged properties such as thrust and discharge current showed very good agreement. However, the same solutions showed relatively poor agreement with measurements of discharge current oscillations. In particular, the simulations predicted higher magnitude oscillations than those observed experimentally.

Subsequent numerical studies investigated the sensitivity of the solutions in the time domain to the numerical parameters and electron mobility models employed. It was found that the results were insensitive to the number of particles employed. Significant sensitivity of the solutions to the time step employed was found, particularly for the three region mobility model. In addition, it was found that the length scales employed by the three-region mobility model affect the way in which the high-frequency mode is captured.

Future work will focus on the development of identifying guidelines that allow solutions to be computed that are independent of the numerical parameters employed. In addition, attempts will be made to modify the three-region electron mobility model to make its solutions less sensitive to numerical parameters. The methods used to simulate the detailed plasma physics within the discharge channel must eventually be improved to result in a more robust response to varying numerical parameters and physical models.

References

[1]Choueiri, E., "Plasma oscillations in Hall thrusters," *Physics of Plasmas*, Vol. 8, No. 4, April 2001, pp. 1411-1426.

[2]Fife, J., *Hybrid-PIC Modeling and Electrostatic Probe Survey of Hall Thruster*, Ph.D. thesis, Massachusetts Institute of Technology, 1998.

[3]Hofer, R.R., Mikellides, I.G., Katz, I., and Goebel, D.M., "BPT-4000 Hall Thruster Discharge Chamber Erosion Model Comparison with Qualification Life Test Data," IEPC-2007-267, *30th International Electric Propulsion Conference*, Florence, Italy, 2007a.

[4]Parra, F., Ahedo, E., Fife, J., and Martinez-Sanchez, M., "A two-dimensional hybrid model of the Hall thruster discharge," *Journal of Applied Physics*, Vol. 100, No. 022304, 2006.

[5]Reid, B., *The Influence of Neutral Flow Rate in the Operation of Hall Thrusters*, Ph.D. thesis, University of Michigan, 2009.

[6]Boyd, I.D., "Review of Hall Thruster Plume Modeling," *Journal of Spacecraft and Rockets,* Vol. 38, No. 3, 2001, pp. 381-387.

[7]Szabo, J., *Fully kinetic numerical modeling of a plasma thruster*, Ph.D. thesis, Massachusetts Institute of Technology, 2001.

[8]Gamero-Castano, M. and Katz, I., "Estimation of Hall Thruster Erosion Using HPHall," 29th International Electric Propulsion Conference, Princeton University, Princeton, 2005.

[9]Parra, F., Escobar, D., and Ahedo, E., "Improvements on particle accuracy in a Hall thruster hybrid code," 42nd AIAA/ASME/SAE/ASEE Joint Propulsion Conference, Sacramento, CA, AIAA 2006-4830, 2006.

[10]Hofer, R.R., Katz, I., Mikellides, I.G., and no, M. G.-C., "Heavy Particle Velocity and Electron Mobility Modeling in Hybrid-PIC Hall Thruster Simulations," 42nd AIAA/ASME/SAE/ASEE Joint Propulsion Conference, Sacramento, CA, AIAA 2006-4658, 2006.

[11]Hofer, R.R., Mikellides, I.G., Katz, I., and Goebel, D.M., "Wall Sheath and Electron Mobility Modeling in Hybrid-PIC Hall Thruster Simulations," 43rd AIAA/ASME/ SAE/ASEE Joint Propulsion Conference, Cincinnati, OH, AIAA 2007-5267, 2007b.

[12]Hofer, R.R., et al., "Efficacy of Electron Mobility Models in Hybrid-PIC Hall Thruster Simulations," 44th AIAA/ASME/SAE/ASEE Joint Propulsion Conference, Hartford, CT, AIAA 2008-4924, 2008.

[13]Hagelaar, et al., "Role of Anomalous Electron Transport in a Stationary Plasma Thruster Simulation," Journal of Applied Physics, Vol. 13, No. 1, 2003, pp. 67-75.

[14]Koo, J.W. and Boyd, I.D., "Modeling of Anomalous Electron Mobility in Hall Thrusters," Physics of Plasmas, Vol. 13, No. 033501, 2006.

[15]James, G. and Lowder, R., "Anomalous Electron Diffusion and Ion Acceleration in a Low-Density Plasma," Physics of Fluids, Vol. 9, No. 1115, 1966.

[16]Nicholson, D.R., Introduction to Plasma Theory, Wiley & Sons, Inc., 1983.